Computerized Medical Imaging and Graphics 35 (2011) 506–514

Contents lists available at ScienceDirect

Computerized Medical Imaging and Graphics

journal homepage: www.elsevier.com/locate/compmedimag

# Computer-aided prognosis: Predicting patient and disease outcome via quantitative fusion of multi-scale, multi-modal data☆

Anant Madabhushi*, Shannon Agner, Ajay Basavanhally, Scott Doyle, George Lee

*Department of Biomedical Engineering, Rutgers University, Piscataway, NJ 08854 United States*

ARTICLE INFO

*Article history:*
Received 26 June 2010
Received in revised form
16 December 2010
Accepted 10 January 2011

*Keywords:*
Computer-aided prognosis (CAP)
Breast cancer
Prostate cancer
Personalized medicine
Digital pathology
Data fusion
Multi-modal
Mass spectrometry
Gleason grade
Outcome
Protein expression

ABSTRACT

Computer-aided prognosis (CAP) is a new and exciting complement to the field of computer-aided diagnosis (CAD) and involves developing and applying computerized image analysis and multi-modal data fusion algorithms to digitized patient data (e.g. imaging, tissue, genomic) for helping physicians predict disease outcome and patient survival. While a number of data channels, ranging from the macro (e.g. MRI) to the nano-scales (proteins, genes) are now being routinely acquired for disease characterization, one of the challenges in predicting patient outcome and treatment response has been in our inability to quantitatively fuse these disparate, heterogeneous data sources. At the Laboratory for Computational Imaging and Bioinformatics (LCIB)[1] at Rutgers University, our team has been developing computerized algorithms for high dimensional data and image analysis for predicting disease outcome from multiple modalities including MRI, digital pathology, and protein expression. Additionally, we have been developing novel data fusion algorithms based on non-linear dimensionality reduction methods (such as Graph Embedding) to quantitatively integrate information from multiple data sources and modalities with the overarching goal of optimizing meta-classifiers for making prognostic predictions. In this paper, we briefly describe 4 representative and ongoing CAP projects at LCIB. These projects include (1) an Image-based Risk Score (IbRiS) algorithm for predicting outcome of Estrogen receptor positive breast cancer patients based on quantitative image analysis of digitized breast cancer biopsy specimens alone, (2) segmenting and determining extent of lymphocytic infiltration (identified as a possible prognostic marker for outcome in human epidermal growth factor amplified breast cancers) from digitized histopathology, (3) distinguishing patients with different Gleason grades of prostate cancer (grade being known to be correlated to outcome) from digitized needle biopsy specimens, and (4) integrating protein expression measurements obtained from mass spectrometry with quantitative image features derived from digitized histopathology for distinguishing between prostate cancer patients at low and high risk of disease recurrence following radical prostatectomy.



## 1. Introduction

Most researchers agree that cancer is a complex disease which we do not yet fully understand. Predictive, preventive, and personalized medicine (PPP) has the potential to transform clinical practice by decreasing morbidity due to diseases such as cancer by integrating multi-scale, multi-modal, and heterogeneous data to determine the probability of an individual contracting certain diseases and/or responding to a specific treatment regimen [3]. In the clinic, the same treatment applied to two patients with diseases that look very similar often have vastly different outcomes under the same treatment [4,5]. A part of this difference is undoubtedly patient specific, but a part must also be a result of our limited understanding of the relationship between disease progression and clinical presentation.

### 1.1. Need for quantitative data fusion in personalized medicine

An understanding of the interplays of different hierarchies of biological information from proteins, tissue, metabolites, and imaging will provide conceptual insights and practical innovations that will profoundly transform people's lives [3,5,6]. There is a consensus among clinicians and researchers that a more quantitative approach, using computerized imaging techniques to better understand tumor morphology, combined with the classification of disease into more meaningful molecular subtypes, will lead to better patient care and more effective therapeutics [5,7,8]. With the advent of digital pathology [5,6,9], multi-functional imaging, mass spectrometry, immuno-histochemical, and fluorescent

[1] http://lcib.rutgers.edu.
☆ A preliminary version of this paper appeared in [1].
* Corresponding author. Tel.: +1 732 445 4500x6213.
*E-mail address:* anantm@rci.rutgers.edu (A. Madabhushi).

0895-6111/$ – see front matter © 2011 Elsevier Ltd. All rights reserved.
doi:10.1016/j.compmedimag.2011.01.008

in situ hybridization (FISH) techniques, the acquisition of multiple, orthogonal sources of genomic, proteomic, multi-parametric radiological, and histological information for disease characterization is becoming routine at several institutions [10,11]. Computerized image analysis and high dimensional data fusion methods will likely constitute an important piece of the prognostic tool-set to enable physicians to predict which patients may be susceptible to a particular disease and also for predicting disease outcome and survival. These tools will also have important implications in theragnostics [12–14], the ability to predict how an individual may react to various treatments, thereby (1) providing guidance for developing customized therapeutic drugs and (2) enabling development of preventive treatments for individuals based on their potential health problems. A theragnostic profile that is a synthesis of various biomarker and imaging tests from different levels of the biological hierarchy (genomic, proteomic, metabolic) could be used to characterize an individual patient and her/his drug treatment outcome.

### 1.2. Challenges to fusion of imaging and non-imaging biological data

If multiple sensors or sources are used in the inference process, in principle, they could be fused at one of 3 levels in the hierarchy; (1) raw data-level fusion, (2) feature-level fusion, or (3) decision-level fusion [15,16]. Several classifier ensemble or multiple classifier schemes have been previously proposed to associate and correlate data at the decision-level (combination of decisions (COD)) [17–24]; a much easier task compared to data integration at the raw-data or feature level (combination of features (COF)). Traditional decision fusion based approaches have focused on combining either binary decisions $\mathcal{Y}_\alpha(c) \in \{+1, -1\}$, ranks, or probabilistic classifier outputs $\mathcal{P}_\alpha(c)$ obtained via classification of each of the $k$ individual data sources $\mathbf{F}_\alpha(c)$, $\alpha \in \{1, 2, \ldots, k\}$, via a Bayesian framework [25], Dempster–Shafer evidence theory [26], fuzzy set theory, or via classical decision ensembles schemes, e.g. Adaboost [19], Support Vector Machines (SVM) [18], or Bagging [17]. At a given data scale (e.g. radiological images such as MRI and CT), several researchers [27–35] have developed techniques for combining imaging data sources (assuming the registration problem has been solved) by simply concatenating the individual image modality attributes $\mathbf{F}_{\text{MRI}}(c)$ and $\mathbf{F}_{\text{CT}}(c)$ at every spatial location $c$ to create a combined feature vector $[\mathbf{F}_{\text{MRI}}(c), \mathbf{F}_{\text{CT}}(c)]$ which can be input to a classifier. However when the individual modalities are heterogeneous (image and non-image based) and of different dimensions, e.g. a 256 dimensional vectorial spectral signal $\mathbf{F}_{\text{MRS}}(c)$ and a scalar image intensity value $\mathbf{F}_{\text{MRI}}(c)$, a simple concatenation $[\mathbf{F}_{\text{MRI}}(c), \mathbf{F}_{\text{MRS}}(c)]$ will not provide a meaningful data fusion solution. Thus, a significant challenge in integrating heterogeneous imaging and non-imaging biological data has been the lack of a quantifiable knowledge representation framework to reconcile cross-modal, cross-dimensional differences in feature values.

While no general theory yet exists for domain data fusion, most researchers agree that heterogeneous data needs be represented in a way that will allow for confrontation of the different channels, an important prerequisite to fusion or classification. Bruno et al. [36] recently designed a multimodal dissimilarity space for retrieval of video documents. Lanckriet et al. [37] and Lewis et al. [38] both presented kernel based frameworks for representing heterogeneous data relating to protein sequences and then used the data representation in conjunction with a SVM classifier [18] for protein structure prediction. Mandic et al. [39] recently proposed a sequential data fusion approach for combining wind measurements via the representation of directional signals within the field of complex numbers. Coppock and Mazlack [40] extended Gower's metric [41] for nominal and ordinal data integration within an agglomerative hierarchical clustering algorithm to cluster mixed data.

In spite of the challenges, data fusion at the feature level aims at retrieving the interesting characteristics of the phenomenon being studied [39]. Kernel-based formulations have been used in combining multiple related datasets (such as gene expression, protein sequence, and protein–protein interaction data) for function prediction in yeast [37] as well as for heterogeneous data fusion for studying Alzheimer's disease [42]. However the selection and tuning of the kernels used in multi-kernel learning (MKL) play an important role in the performance of the approach. This selection proves to be non-trivial when considering completely heterogeneous, multi-scale data such as molecular protein-, and gene-expression signatures and imaging and metabolic phenotypes. Additionally these methods typically employ the same kernel or metric, across modalities, for estimating object similarity. Thus while the Euclidean kernel might be appropriate for image intensities, it might not be appropriate for all feature spaces (e.g. time series spectra or gene expression vectors) [43].

### 1.3. Use of non-linear dimensionality reduction methods for uniformly representing multi-modal data

Recently, approaches involving the use of dimensionality reduction (DR) methods for representing high dimensional data in terms of embedding vectors in a reduced dimensional space have been proposed. Applications have included the fusion of heterogeneous dimensional data (e.g. scalar imaging (MRI) and vectorial information (e.g. magnetic resonance spectroscopy (MRS))) [44–46] by attempting to reduce the dimensionality of the higher dimensional data source to that of the lower dimensional modality via principal component analysis (PCA), independent component analysis (ICA), or a linear combination model (LCM) [47]. However, these strategies often lead to non-optimal fusion solutions due to (a) use of linear DR schemes, (b) dimensionality reduction of only the non-imaging data channel and (c) large scaling differences between the different modalities. Yu and Tresp proposed a generalized PCA model for representing real-world image painting data [48]. Recently, manifold learning (ML) methods such as isometric mapping (Isomap) [49] and locally linear embedding (LLE) [50] have become popular for mapping high dimensional information into a low dimensional representation for the purpose of visualization or classification. While these non-linear DR (NLDR) methods enjoy advantages compared to traditional linear DR methods such as PCA [51] and LCM [52] in that they are able to discover non-linear relationships in the data [53,54], they are notoriously susceptible to the choice of optimal embedding parameters [49,50].

Researchers have since been developing novel methods for overcoming the difficulties in obtaining an appropriate manifold representation of the data. Samko et al. [55] has developed an estimator for optimal neighborhood size for Isomap. However, in cases of varying neighborhood densities, an optimal neighborhood size may not exist on a global scale. Others have developed adaptive methods that select neighbors based on additional constraints such as local tangents [56,57], intrinsic dimensionality [58], and estimating geodesic distances within a neighborhood [59]. The additional constraints in these adaptive methods aim to create a graph that does not contain spurious neighbors, but the use of additional constraints leaves the user with an additional degree of freedom to define when creating a manifold.

Along with other groups [60–62], *the Rutgers Laboratory for Computational Imaging and Bioinformatics (LCIB) group has been working on developing* NLDR schemes that have been shown to be more resistant to some of the failings of LLE [50] and Isomap [49]. C-Embed is a consensus NLDR scheme that [54,63–65] combines multiple low dimensional multi-dimensional projections of the data to obtain a more robust low dimensional data representation, one which is not sensitive to careful selection of the neighborhood

parameter ($\kappa$), unlike LLE and Isomap. These schemes [11,63,65–69] allow for non-linearly transforming each of the $k$ individual high dimensional heterogeneous modalities into the common format of low dimensional embedding vectors thereby enabling direct, data-level fusion of structural, functional, metabolic, architectural, genomic, and proteomic information in the original space while overcoming the differences in scale, size, and dimensionality of individual feature spaces. This integrated representation of multiple modalities in the transformed space can be used to train meta-classifiers for studying and predicting biological activity.

### 1.4. Need to identify markers of aggressive disease

While a diagnostic marker identifies diseased from normal tissue, a *prognostic* marker identifies subgroups of patients associated with different disease outcomes. With increasing early detection of diseases via improved diagnostic imaging methodologies [21,64,65,69–73], it has become important to predict biologic behaviors and disease "aggressiveness". Clinically applicable prognostic markers are urgently needed to assist in the selection of optimal therapy. In the context of prostate cancer (PCa), well established prognostic markers include histologic grade, prostate specific antigen (PSA), margin positivity, pathologic stage, intraglandular tumor extent, and DNA ploidy [74–76]. Other recently promising prognostic indicators include tumor suppressor gene p53, cell proliferation marker Ki-67, Oncoantigen 519, microsatellite instability, angiogenesis and tumor vascularity (TVC), vascular endothelial growth factor (VEGF), and E-cadherin [76,77]. None of these factors, however, have individually proven to be accurate enough to serve routinely as a prognostic marker [77,78]. The problem is that men with early detected PCa have in 50% of cases [79], and in some cases 80% [80], a homogeneous pattern with respect to most standard prognostic variables (PSA < 10, T1c, Gleason score < 7). In this growing group of patients, the traditional markers seem to lose their efficacy and the subsequent therapy decision is complicated. Gao et al. [81] suggest that only a combination of multiple prognostic markers will prove superior to any individual marker. Graefen et al. [82] and Stephenson et al. [83–85] have suggested that better prognostic accuracy can be obtained by a combination of the individual markers via a machine classifier like an artificial neural network.

### 1.5. Graph based features to characterize spatial arrangement of nuclear structures

Graphs are effective techniques to represent *spatial arrangement of structures* by defining a large set of topological features. These features are quantified by definition of computable metrics. The use of spatial-relation features for quantifying cellular arrangement was proposed in the early 1990s [86,87], but did not find application to biomedical imagery until recently [88–94]. However, with recent evidence demonstrating that for certain classes of tumors, tumor–host interactions correlate with clinical outcome [95], graph algorithms clearly have a role to play in modeling the tumor–host network and hence in predicting disease outcome.

Table 1 lists common spatial, graph based features that one can extract from the Voronoi Diagram (VD), Delaunay Triangulation (DT), and the Minimum Spanning Tree (MST) [96–98]. Additionally a number of features based off nuclear statistics can be similarly extracted. Using the nuclear centroids in a tissue region (Fig. 1(a)) as vertices, the DT graph (Fig. 1(b)), a unique triangulation of the centroids, and the MST (Fig. 1(c)), a graph that connects all centroids with the minimum possible graph length, can be constructed. These features quantify important biological information, such as the proliferation and structural arrangement of the cells in the tissue, which is closely tied to cancerous activity. Our hypothesis is that the genetic descriptors that define clinically relevant classes of cancer are reflected in the visual characteristics of the cellular morphology and tissue architecture, and that these characteristics can be measured by image analysis techniques. *We believe that image-based classifiers of disease developed via comprehensive analysis of quantitative image-based information present in tissue histology will have strong correlation with gene-expression based prognostic classification*.

### 1.6. Ongoing Projects at the Laboratory for Computational Imaging and Bioinformatics (LCIB)

At LCIB in Rutgers University, we have been developing an array of computerized image analysis and high dimensional data analysis, fusion tools for quantitatively integrating molecular features of a tumor (as measured by gene expression profiling or mass spectrometry) [54,99], results from the imaging of the tumor cellular architecture and microenvironment (as captured in histological imaging) [6,9], the tumor 3-d tissue architecture [100], and its metabolic features (as seen by metabolic or functional imaging modalities such as Magnetic Resonance Spectroscopy (MRS)) [21,64,65,69–73]. In this paper, we briefly describe 4 representative and ongoing projects at LCIB in the context of predicting outcome of breast and prostate cancer patients and involving computerized image, data analysis and fusion of quantitative measurements from digitized histopathology, and protein expression features obtained via mass spectrometry. Preliminary data pertaining to these projects is also presented.

## 2. Image-based risk score for ER+ breast cancers

The current *gold standard* for achieving a quantitative and reproducible prognosis in estrogen receptor-positive breast cancers (ER+ BC) is via the Oncotype DX (Genomic Health, Inc.) molecular assay, which produces a Recurrence Score (RS) between 0 and 100, where a high RS corresponds to a poor outcome and vice versa. In [101], we presented Image-based Risk Score (IbRiS), a novel CAP scheme that uses only quantitatively derived information (architectural features derived from spatial arrangement of cancer nuclei) from digitized ER+ BC biopsy specimens (Fig. 1(a)) to help clinicians predict which ER+ BC patients have more aggressive disease and consequently need adjuvant chemotherapy over and above standard hormonal therapy. The hypothesis behind IbRiS is that quantitative image features can be used to implicitly model tumor grade which is known to be correlated with outcome in ER+ BC total of 25 architectural features, derived from the DT and MST graphs are extracted (using the nuclear centers as graph vertices). These features quantify the area and perimeter of triangles in the DT and branch lengths in the MST (Table 1). Graph Embedding [102], a non-parametric NLDR technique, is employed to project the features onto a reduced 3D space while simultaneously preserving object-class relationships. This allows us to observe the discriminability of the architectural features with respect to low and high RS on a smooth, continuous manifold (Fig. 2(a)). The 3D embedding is subsequently unraveled into a normalized 1D IbRiS scale (Fig. 2(b)). With a large enough cohort of annotated data, prognostic thresholds $\theta_1$ and $\theta_2$ could be learnt and employed for making prognostic predictions of outcome.

The separation between samples with high and low RS (Fig. 2(a)) is reflected quantitatively by the classification accuracy >84% [101] of a SVM classifier. Furthermore, by re-labeling the samples into three classes of low, intermediate, and high RS (Fig. 2(b)) we are able to qualitatively confirm that the variations in phenotype described by the architectural features are truly representative of the underlying differences in genotype that affect disease outcome.

**Table 1**
A breakdown of 50 architectural features used for quantification of spatial arrangement of nuclei in histopathology images, comprising 25 graph-based and 25 nearest neighbor features.

| Feature set | Description | # of features |
|---|---|---|
| Voronoi Diagram (VD) | Total area of all polygons, polygon area, polygon perimeter, polygon chord length | 13 |
| Delaunay Triangulation (DT) | Triangle side length, triangle area | 8 |
| Minimum Spanning Tree (MST) | Edge length | 4 |
| Nuclear statistics (nearest neighbor) | Density of nuclei, distance to {3, 5, 7} nearest nuclei, nuclei in {10, 20, . . ., 50} pixel radius | 25 |

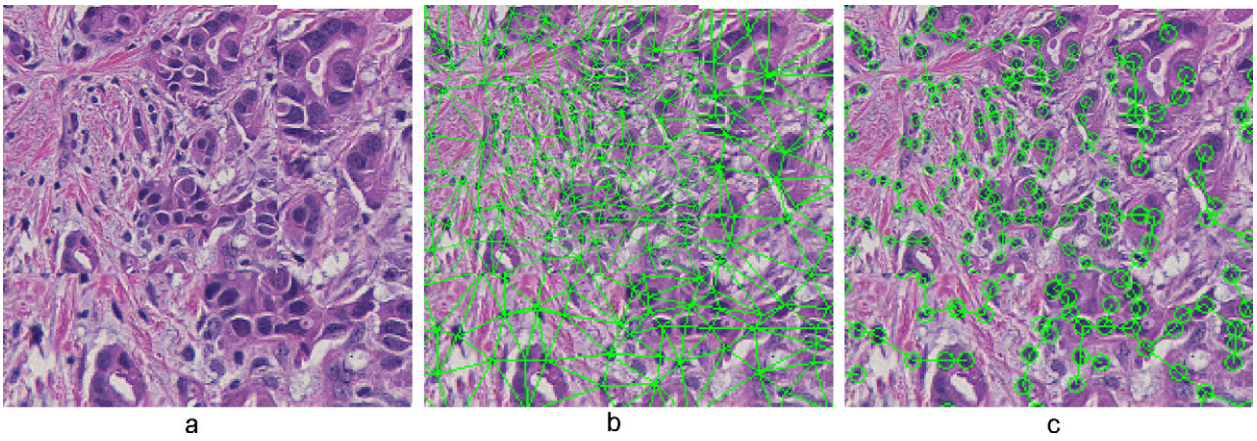


**Fig. 1.** Nuclear centroids from an (a) ER+ BC histopathology image are used to construct associated (b) Delaunay Triangulation and (c) Minimum Spanning Tree graphs. A total of 12 architectural features are extracted from these graphs and used to quantitatively model phenotypic appearance and hence implicitly the grade of ER+ BC biopsy specimen.

## 3. Lymphocytic infiltration and outcome in HER2+ breast cancers

The identification of phenotypic changes in BC histopathology with respect to corresponding molecular changes is of significant clinical importance in predicting BC outcome. One such example is the presence of lymphocytic infiltration (LI) in BC histopathology, which has been correlated with nodal metastasis and distant recurrence in human epidermal growth factor amplified (HER2+) breast cancers.

In [103,104], we introduced a computerized image analysis system for detecting and grading the extent of LI in a digitized HER2+ BC biopsy image. The methodology comprised a region-growing scheme to automatically segment all nuclei (lymphocytic and non-lymphocytic) within the image. The segmentation was then refined via Maximum *a Posteriori* estimation, which utilizes (1) size and intensity information to isolate lymphocytic nuclei and (2) Markov Random Fields [9] to separate clusters of LI from the surrounding baseline level of immune response. The centroids of the resulting lymphocytic nuclei are used to construct graphs (VD, DT, MST) and a total of 50 architectural features are extracted from each histopathology image (Table 1). The features are reduced to a 3D embedding space via Graph Embedding. Fig. 3 shows that the low dimensional representation (obtained via Graph Embedding) of HER2+ BC histopathology images from which Voronoi graph based features were derived to quantitatively characterize the extent, pattern, and density of LI (presence of lymphocytic nuclei), results in a smooth curvilinear manifold with a continuous transition from low to intermediate to high levels of LI (levels of LI have been clinically correlated to disease outcome – high levels of LI result in better outcome/survival) [105]. By mapping new samples onto this manifold and based on the location of the sample on the manifold, a prediction of disease outcome could be made. The manifold in the meta-space captures the biological transformation of the disease in its transition from good to poor prognosis cancer. In conjunction with the architectural features, a SVM classifier was able to successfully distinguish samples with different levels of LI extent at >90% classification accuracy [104] (the ground truth for LI extent was identified by an expert clinician as being either high, intermediate, or low for each histology image).

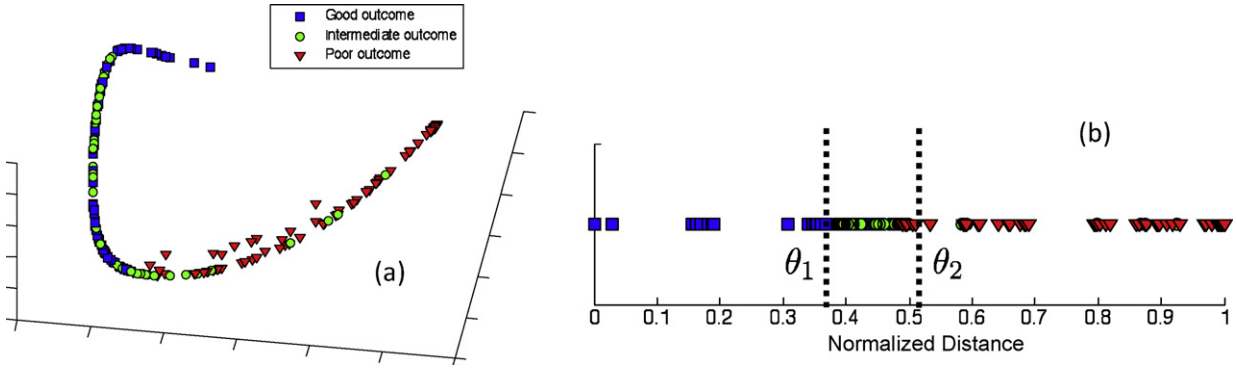


**Fig. 2.** 37 ER+ histopathology images are plotted in (a) a 3D Graph Embedding space created by reducing the 25 architectural features. The embedding is linearized into (b) the 1D IbRiS scale. Overlaying Recurrence Score labels allows us to identify prognostic thresholds $\theta_1$ and $\theta_2$ for distinguishing poor and good outcome ER+ BC's.

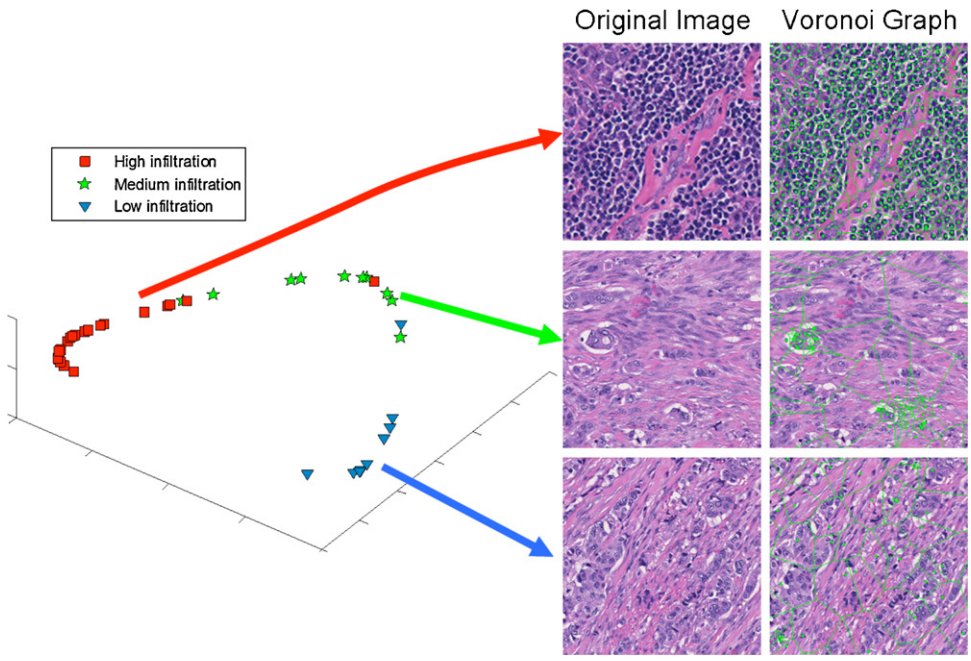


**Fig. 3.** Visualization of HER2+ BC tissue samples with low-, to medium-, to high-levels of lymphocytic infiltration (LI) [1–3] in the meta-space. Graphs constructed on the LI allows for extraction of architectural features, resulting in a smooth manifold (obtained via C-Embed) with clear separation between different LI levels.

## 4. Automated Gleason grading on prostate cancer histopathology

PCa is diagnosed in over 200,000 people and causes 27,000 deaths in the US annually. However, the five-year survival rate for patients diagnosed at an early stage of tumor development is very high [106,107]. If PCa is found on a needle biopsy, the tumor is then assigned a Gleason grade (1–5) [6,9]. Gleason grade 1 tissue is highly differentiated and non-infiltrative while grade 5 is poorly differentiated and highly infiltrative. Gleason grading is predominantly based on tissue architecture (spatial arrangement of nuclei and glands) and tumor morphology (shape and size of glands and

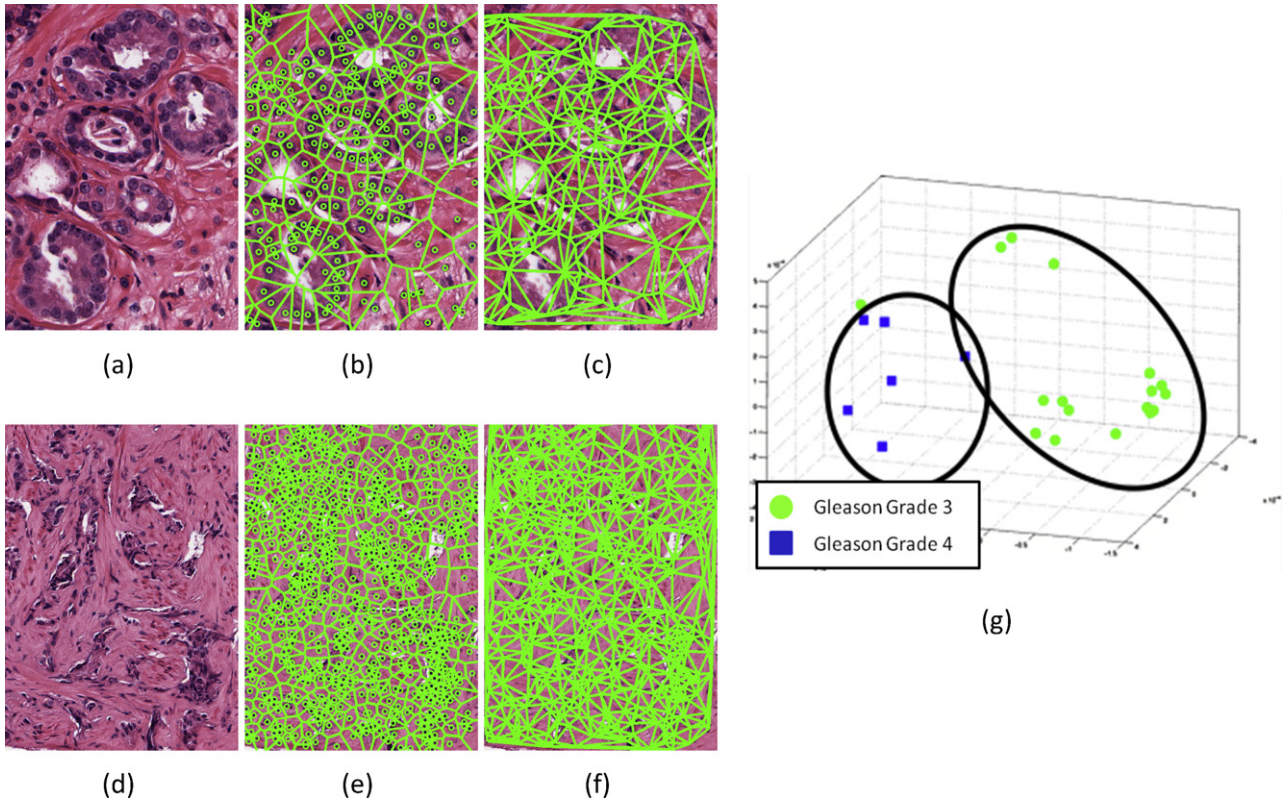


**Fig. 4.** Gleason grade (a–c) 3 and (d–f) 4, prostate cancer biopsy specimens. Voronoi (b), (e) and Delaunay (c), (f) graph-based features quantify spatial architecture of the tissues. The results of applying Graph Embedding to these image descriptors is shown in (g). Note the excellent separation between grades 3 (circles) and 4 (squares) in (g).

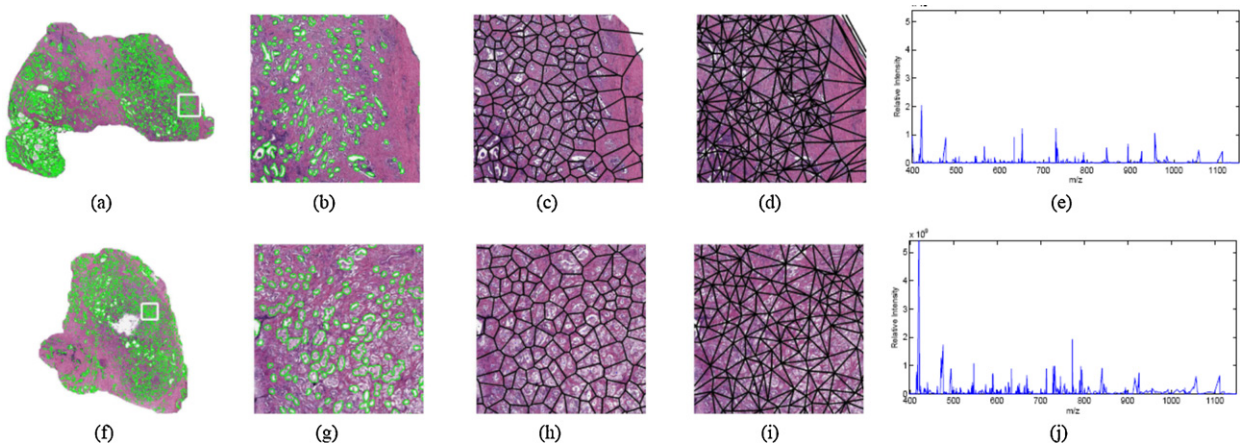


**Fig. 5.** Regions of interest (a, f) identified (segmented glands) by our PPMM + HNCuts [2] scheme (and validated by a pathologist) for extracting a sample of the prostate tumor for mass spectrometry analysis (e, j). An adjacent slice is used to examine the architectural (c, d, h, i) image features (see Table 1) from the prostate. The top row corresponds to a gland from a relapsed patient, and the bottom row corresponds to a relapse-free patient.

nuclei). As tissue regions transform from (a) benign to malignant, and (b) tumor regions transform from lower to higher grades, the architecture and morphology of the images undergo significant changes: nuclear proliferation and infiltration increase, glands in the prostate tissue become smaller, circular, and uniform, and the overall texture of the tissue is altered. Since Gleason grade is known to be strongly correlated to disease outcome, accurately distinguishing between different Gleason grades is critical for making treatment decisions. While pathologists are able to reliably distinguish between low and high Gleason grades (1 and 5), there is a great deal more inter-, and intra-observer variability when it comes to distinguishing intermediate Gleason 3 and 4 patterns (see Fig. 4(a) and (d)).

At LCIB, we have developed a PCa system that employs morphological, architectural (Table 1), and textural features derived from prostate needle biopsy specimens [108] to distinguish intermediate Gleason patterns. These features include information traditionally used in the Gleason grading paradigm (morphology and nuclear density) as well as features not considered by pathologists (such as second-order co-adjacency and global texture features). By employing these features in conjunction with a SVM classifier, we were able to distinguish between 40 samples of Gleason grades 3 and 4 with an accuracy of 96.2%. Fig. 4(g) illustrates these results, where each point on the scatter plot represents a PCa biopsy sample (Gleason grade 3 shown with green circles while Gleason grade 4 samples as blue squares). The distance between any two samples is related to their similarity in the original, high dimensional feature space; samples that cluster together have similar feature values and likely to belong to the same Gleason pattern.

## 5. Integrated proteomic, histological signatures for predicting prostate cancer recurrence

Following radical prostatectomy (RP), there remains a substantial risk of disease recurrence (estimated at 25–40%) [109]. Studies have identified infiltration beyond the surgical margin, and high Gleason score as possible predictors of prostate cancer recurrence. However, owing to inter-observer variability in Gleason grade determination, cancers identified with the same Gleason grade could have significantly different outcomes [110]. Discovery of a predictive biomarker for outcome following RP would allow for therapeutic intervention if the patient was found to have poor prognosis. Protein expression features of excised prostate tissue may add complementary prognostic information to standard morphologic and architectural features derived from histopathology [111].

In [99], we attempted to integrate morphological and architectural features (Table 1) quantitatively extracted from digitized excised prostate specimens along with protein expression measurements obtained via electrospray mass spectrometry from the dominant tumor nodule; the idea being to develop an integrated prognostic meta-marker for predicting disease recurrence following RP (Fig. 5). To accommodate two widely different modalities (imaging and proteomics), we developed the Generalized Fusion

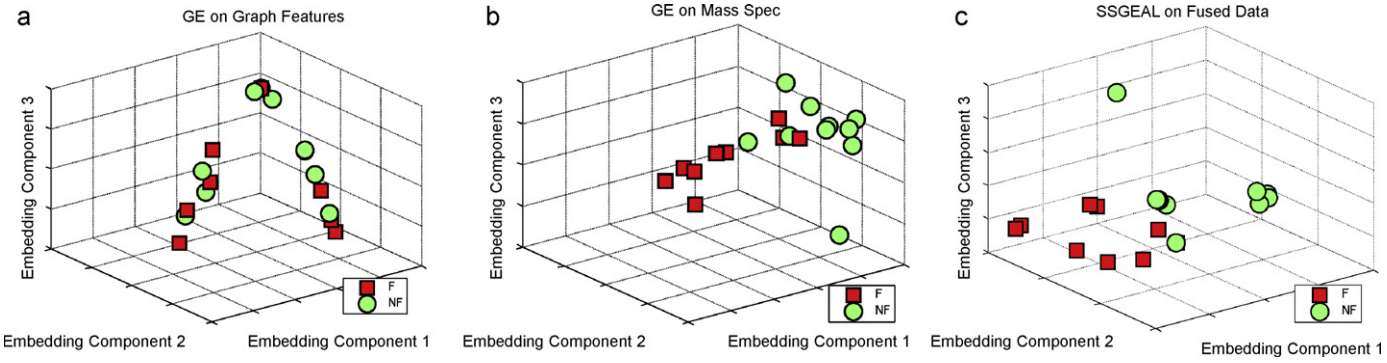


**Fig. 6.** Preliminary fusion results using the knowledge representation framework to distinguish between a total of 25 progressors (squares) and non-progressors (circles). In (a)–(c), respectively are shown the meta-space embedding results obtained using (a) histological image features alone, (b) peptide features alone, and (c) the fused histo-proteomics feature set.

Framework (GFF) for homogeneously representing each of the data types in a normalized, and dimensionality compatible meta-space representation prior to classification in the fused space.

Greater separation between prostate cancer recurrence (red squares) and non-recurrence (green circles) cases was observed in the combined morphologic, architectural, proteomic space (Fig. 6(c)) compared to the individual modality spaces (Fig. 6(a) and (b)). These results appear to suggest that inclusion of complementary proteomic measurements with traditional Gleason grading based morphologic and architectural measurements may allow for improved prediction of PCa recurrence following RP.

## 6. Concluding remarks

In this paper we briefly described some of the primary challenges in the quantitative fusion of multi-scale, multi-modal data for building prognostic meta-classifiers for predicting treatment response and patient outcome. We also described some of the ongoing efforts at the Laboratory for Computational Imaging and Bioinformatics (LCIB) at Rutgers University to address some of these computational challenges in personalized therapy and highlighted ongoing projects in computer-aided prognosis of breast and prostate cancer. Other groups such as Cooper et al. [112] are applying similar techniques to predicting survival outcome in the context of follicular lymphomas. Further developments in this area will only come about by close and dedicated interactions between computer and imaging scientists, clinicians, oncologists, radiologists, and pathologists.

## Acknowledgments

This work was supported by the Wallace H. Coulter Foundation, the National Cancer Institute under Grants R01CA136535, R01CA140772, R03CA143991, the Cancer Institute of New Jersey, and the Department of Defense (W81XWH-08-1-0145).

## References

[1] Madabhushi A, Basavanhally A, Doyle S, Agner S, Lee G. Computer-aided prognosis: predicting patient and disease outcome via multi-modal image analysis. IEEE Int Symp Biomed Imaging (ISBI) 2010:1415–8.
[2] Janowczyk A, Chandran S, Singh R, Sasaroli D, Coukos G, Feldman MD, et al. Hierarchical normalized cuts: unsupervised segmentation of vascular biomarkers from ovarian cancer tissue microarrays. Med Image Comput Comput Assist Interv 2009;12:230–8.
[3] Madabhushi A, Doyle S, Lee G, Basavanhally A, Monaco J, Masters S, et al. Integrated diagnostics: a conceptual framework with examples, Clinical Chemistry and Laboratory Medicine. Clin Chem Lab Med 2010;48:989–98.
[4] Madabhushi A. Digital pathology image analysis: opportunities and challenges. Imaging Med 2009;1:7–10.
[5] Agner S, Madabhushi A, Rosen M, Schnall M, Nosher J, Somans S, et al. A comprehensive multi-attribute manifold learning scheme-based computer aided diagnostic system for breast MRI. In: SPIE medical imaging. 2008.
[6] Doyle S, Tomaszewski J, Feldman M, Madabhushi A. A boosted Bayesian multi-resolution classifier for prostate cancer detection from digitized needle biopsies. IEEE Trans Biomed Eng 2010.
[7] Madabhushi A, Shi J, Rosen M, Tomaszeweski J, Feldman M. Graph embedding to improve supervised classification: detecting prostate cancer. In: Medical image computing and computer assisted intervention. Palm Springs, vol. 3749. CA: Springer Verlag; 2005. p. 729–38.
[8] Lenkinski RE, Bloch BN, Liu F, Frangioni JV, Perner S, Rubin MA, et al. An illustration of the potential for mapping MRI/MRS parameters with genetic over-expression profiles in human prostate cancer. Magma 2008;21(November):411–21.
[9] Monaco J, Tomaszweski J, Feldman M, Moradi M, Mousavi P, Boag A, et al. Pairwise probabilistic models for markov random fields: detecting prostate cancer from digitized whole-mount histopathology. Med Image Anal 2010;14:617–29.
[10] Juan D, Alexe G, Antes T, Liu H, Madabhushi A, Delisi C, et al. Identification of a MicroRNA panel for clear-cell kidney cancer. Urology 2009;24(Decmber).
[11] Lexe G, Monaco J, Doyle S, Basavanhally A, Reddy A, Seiler M, et al. Towards improved cancer diagnosis and prognosis using analysis of gene expression data and computer aided imaging. Exp Biol Med (Maywood) 2009;234(August):860–79.
[12] Pene F, Courtine E, Cariou A, Mira JP. Toward theragnostics. Crit Care Med 2009;37(January):S50–8.
[13] Lippi G. Wisdom of theragnostics, other changes. MLO Med Lab Obs 2008;40(January):6.
[14] Ozdemir V, Williams-Jones B, Cooper DM, Someya T, Godard B. Mapping translational research in personalized therapeutics: from molecular markers to health policy. Pharmacogenomics 2007;8(February): 177–85.
[15] Mirza AR. An architectural selection framework for data fusion in sensor platforms. In: Systems design and management program. MS Boston: Massachusetts Institute of Technology; 2006. p. 102.
[16] Hall DL. Perspectives on the fusion of image and non-image data. In: AIPR. 2003.
[17] Breiman L. Bagging predictors. Mach Learn 1996;24:123–40.
[18] Burges CA. Tutorial on support vector machines for pattern recognition. Data Min Knowl Discov 1998;2:121–67.
[19] Freund RSY. Experiments with a new boosting algorithm in proceedings of national conference. Mach Learn 1996:148–56.
[20] Madabhushi A, Feldman M, Metaxas D, Chute D, Tomaszeweski J. Optimally combining 3D texture features for automated segmentation of prostatic adenocarcinoma from high resolution MR images. In: IEEE international conference of engineering in medicine and biology society Cancun. 2003. p. 614–7.
[21] Madabhushi A, Feldman M, Metaxas D, Tomaszeweski J, Chute D. Automated detection of prostatic adenocarcinoma from high resolution ex vivo MRI. IEEE Trans Med Imaging 2005;24:1611–25.
[22] Madabhushi A, Shi J, Rosen M, Tomaszeweski J, Feldman M. Comparing classification performance of feature ensembles: detecting prostate cancer from high resolution MRI. Computer vision methods in medical image analysis (in conjunction with ECCV), vol. 4241. Springer Verlag; 2006. p. 25–36.
[23] Twellmann T, Saalbach A, Gerstung O, Leach MO, Nattkemper TW. Image fusion for dynamic contrast enhanced magnetic resonance imaging. Biomed Eng Online 2004;3:35.
[24] Jesneck JL, Nolte LW, Baker JA, Floyd CE, Lo JY. Optimized approach to decision fusion of heterogeneous data for breast cancer diagnosis. Med Phys 2006;33(August):2945–54.
[25] Duda PEHRO. Pattern classification and scene analysis. New York: Wiley; 1973.
[26] Smeulders AW, van Ginneken AM. An analysis of pathology knowledge and decision making for the development of artificial intelligence-based consulting systems. Anal Quant Cytol Histol 1989;11(June):154–65.
[27] Cizek J, Herholz K, Vollmar S, Schrader R, Klein J, Heiss WD. Fast and robust registration of PET and MR images of human brain. Neuroimage 2004;22(May):434–42.
[28] Dube S, El-Saden S, Cloughesy TF, Sinha U. Content based image retrieval for MR image studies of brain tumors. Conf Proc IEEE Eng Med Biol Soc 2006;1:3337–40.
[29] Heckemann RA, Hajnal JV, Aljabar P, Rueckert D, Hammers A. Multiclassifier fusion in human brain MR segmentation: modelling convergence. Med Image Comput Comput Assist Interv Int Conf 2006;9:815–22.
[30] Hunsche S, Sauner D, Maarouf M, Lackner K, Sturm V, Treuer H. Combined X-ray and magnetic resonance imaging facility: application to image-guided stereotactic and functional neurosurgery. Neurosurgery 2007;60(April):352–60 [discussion 360-1].
[31] Liu T, Li H, Wong K, Tarokh A, Guo L, Wong ST. Brain tissue segmentation based on DTI data. Neuroimage 2007;38(October):114–23.
[32] Mascott CR, Summers LE. Image fusion of fluid-attenuated inversion recovery magnetic resonance imaging sequences for surgical image guidance. Surg Neurol 2007;67(June):589–603 [discussion 603].
[33] Rohlfing T, Pfefferbaum A, Sullivan EV, Maurer CR. Information fusion in biomedical image analysis: combination of data vs. combination of interpretations. Inf Process Med Imaging 2005;19:150–61.
[34] Wong TZ, Turkington TG, Hawk TC, Coleman RE. PET and brain tumor image fusion. Cancer J 2004;10(July–August):234–42.
[35] Bloch I, Geraud T, Maitre H. Representation and fusion of heterogeneous fuzzy information in the 3D space for model-based structural recognition – application to 3D brain imaging. Artif Intell 2003;148:141–75.
[36] Bruno E, Moenne-Loccoz N, Marchand-Maillet S. Design of multimodal dissimilarity spaces for retrieval of video documents. IEEE Trans Pattern Anal Mach Intell 2008;30(September):1520–33.
[37] Lanckriet GR, Deng M, Cristianini N, Jordan MI, Noble WS. Kernel-based data fusion and its application to protein function prediction in yeast. Pac Symp Biocomput 2004:300–11.
[38] Lewis DP, Jebara T, Noble WS. Support vector machine learning from heterogeneous data: an empirical analysis using protein sequence and structure. Struct Bioinform 2006;22:2753–60.
[39] Mandic DP, Goh SL. Sequential data fusion via vector spaces: fusion of heterogeneous data in the complex domain. J VLSI Signal Process 2007;48: 99–108.
[40] Coppock S, Mazlack LJ.Multi-modal data fusion: a description. Lecture notes in computer science, vol. 3214. Berlin/Heidelberg: Springer; 2004. p. 1136–42.
[41] Friston KJ, Frith CD, Fletcher P, Liddle PF, Frackowiak RS. Functional topography: multidimensional scaling and functional connectivity in the brain. Cereb Cortex 1996;6(March–April):156–64.

[42] Ye J, Chen K, Wu T, Li J, Zhao Z, Patel R. Heterogeneous data fusion for alzheimer's disease study. In: Proceeding of the 14th ACM SIGKDD international conference on knowledge discovery and data mining. 2008.
[43] Rao S, Rodriguez A, Benson G. Evaluating distance functions for clustering tandem repeats. Genome Inform 2005;16:3–12.
[44] Simonetti AW, Melssen WJ, Szabo de Edelenyi F, van Asten JJ, Heerschap A, Buydens LM. Combination of feature-reduced MR spectroscopic and MR imaging data for improved brain tumor classification. NMR Biomed 2005;18(February):34–43.
[45] Devos A, Simonetti AW, van der Graaf M, Lukas L, Suykens JA, Vanhamme L, et al. The use of multivariate MR imaging intensities versus metabolic data from MR spectroscopic imaging for brain tumour classification. J Magn Reson 2005;173(April):218–28.
[46] Simonetti AW, Melssen WJ, van der Graaf M, Postma GJ, Heerschap A, Buydens LM. A chemometric approach for brain tumor classification using magnetic resonance imaging and spectroscopy. Anal Chem 2003;75(October (15)):5352–61.
[47] Provencher SW. Estimation of metabolite concentrations from localized in vivo proton NMR spectra. Magn Reson Med 1993;30(December):672–9.
[48] Yu K, Tresp V. Heterogenous data fusion via a probabilistic latent-variable model. In: ARCS. 2004. p. 20–30.
[49] Tenenbaum VDSAJCLJB. A global geometric framework for nonlinear dimensionality reduction. Science 2000;290:2319–23.
[50] Roweis ST, Saul LK. Nonlinear dimensionality reduction by locally linear embedding. Science 2000;290:2323–6.
[51] Jolliffe IT. Principal component analysis. New York: Springer-Verlag; 1986.
[52] Duda R, Hart P, Stork D. Pattern classification. John Wiley & Sons, Inc.; 2001.
[53] Lee G, Rodrigues C, Madabhushi A. An empirical comparison of dimensionality reduction methods for classifying gene protein expression datasets. International symposium on bioinformatics research applications, vol. 4463. Atlanta GA: LNBI; 2007. p. 170–81.
[54] Lee G, Rodrigues C, Madabhushi A. Investigating the efficacy of nonlinear dimensionality reduction schemes in classifying gene- and protein-expression studies. IEEE/ACM Trans Comput Biol Bioinform 2008;5: 1–17.
[55] Samko O, Marshall AD, Rosin PL. Selection of the optimal parameter value for the Isomap algorithm. Pattern Recogn Lett 2006;27:968–79.
[56] Wang J, Zhang Z, Zha H. Adaptive manifold learning. NIPS 2004.
[57] Jia W, Hong P, Yi-Shen L, Zhi-Mao H, Jia-Bing W. Adaptive neighborhood selection for manifold learning. Int Conf Mach Learn Cybern 2008:380–4.
[58] Mekuz N, Tsotsos J. Parameterless Isomap with adaptive neighborhood selection. Pattern Recogn 2006:364–73.
[59] Wen G, Jiang L, Wen J. Using locally estimated geodesic distance to optimize neighborhood graph for isometric data embedding. Pattern Recogn 2008;41:2226–36.
[60] Rajpoot DK, Gomez A, Tsang W, Shanberg A. Ureteric and urethral stenosis: a complication of BK virus infection in a pediatric renal transplant patient. Pediatr Transpl 2007;11(June):433–5.
[61] Polzlbauer G, Lidy T, Rauber A. Decision manifolds – a supervised learning algorithm based on self-organization. IEEE Trans Neural Netw 2008;19:1518–30.
[62] Angot F, Clouard R, Elmoataz A, Revenu M. Neighborhood graphs and image processing. SPIE, vol. 2785. 1996. p. 12–23.
[63] Amod Jog AJ, Chandran S, Madabhushi A. Classifying ayurvedic pulse diagnosis via concensus locally linear embedding. In: Biosignals. 2009. p. 388–95.
[64] Tiwari P, Rosen M, Madabhushi A. Consensus-locally linear embedding (C-LLE): application to prostate cancer detection on magnetic resonance spectroscopy. Med Image Comput Comput Assist Interv Int Conf Med Image Comput Comput Assist Interv 2008;11:330–8.
[65] Viswanath S, Madabhushi A, Rosen M. A consensus embedding approach for segmentation of high resolution in vivo prostate magnetic resonance imagery. In: SPIE medical imaging. 2008.
[66] Lee G, Monaco J, Doyle S, Master S, Feldman M, Tomaszewski J, et al. A knowledge representation framework for integrating multi-modal, multi-scale imaging and non-imaging data: predicting prostate cancer recurrence by fusing mass spectrometry and histology. In: IEEE Int Symp Biomed Imaging (ISBI). 2009. p. 77–80.
[67] Tiwari P, Rosen M, Galen P, Kurhanewicz J, Madabhushi A. Spectral Embedding based Probabilistic boosting Tree (ScEPTre): classifying high dimensional heterogeneous biomedical data. In: Medical image computing and computer assisted intervention. 2009. p. 844–51.
[68] Tiwari P, Rosen M, Madabhushi A. Consensus-locally linear embedding (C-LLE): application to prostate cancer detection on magnetic resonance spectroscopy. Med Image Comput Comput Assist Interv 2008;11:330–8.
[69] Viswanath S, Tiwari P, Madabhushi A, Rosen M. A meta-classifier for detecting prostate cancer by quantitative integration of in vivo magnetic resonance spectroscopy magnetic resonance imaging. In: SPIE medical imaging. 2008.
[70] Bloch BN, Furman-Haran E, Helbich TH, Lenkinski RE, Degani H, Kratzik C, et al. Prostate cancer: accurate determination of extracapsular extension with high-spatial-resolution dynamic contrast-enhanced and T2-weighted MR imaging-initial results. Radiology 2007;245(October):176–85.
[71] Tiwari P, Madabhushi A, Rosen M. A hierarchical unsupervised spectral clustering scheme for detection of prostate cancer from magnetic resonance spectroscopy (MRS). In: Medical image computing and computer assisted intervention, vol. 4792. Brisbane Australia: 2007. p. 278–286.
[72] Viswanath S, Chappelow J, Toth R, Rofsky N, Lenkinski R, Genega E, et al. An integrated segmentation, registration, and cancer detection scheme on 3 Tesla in vivo prostate DCE MRI. In: Medical image computing and computer assisted intervention 2008; accepted for publication.
[73] Viswanath S, Bloch BN, Rosen M, Chappelow J, Rofsky N, Lenkinski R, et al. Integrating structural and functional imaging for computer assisted detection of prostate cancer on multi-protocol in vivo 3 Tesla MRI. In: SPIE medical imaging. 2009.
[74] Bostwick DG. Grading prostate cancer. Am J Clin Pathol 1994;102(October):S38–56.
[75] Djavan B, Kadesky K, Klopukh B, Marberger M, Roehrborn CG. Gleason scores from prostate biopsies obtained with 18-gauge biopsy needles poorly predict Gleason scores of radical prostatectomy specimens. Eur Urol 1998;33:261–70.
[76] Ito K, Nakashima J, Mukai M, Asakura H, Ohigashi T, Saito S, et al. Prognostic implication of microvascular invasion in biochemical failure in patients treated with radical prostatectomy. Urol Int 2003;70:297–302.
[77] Gao X, Porter A, Grignon D, Pontes J, Honn K. Diagnostic and prognostic markers for human prostate cancer. Prostate 1997;31:264–81.
[78] Khatami A. Early prostate cancer: on prognostic markers and predictors of treatment outcome and radical prostaectomy. Gothenburg: Intellecta DocuSys AB; 2007.
[79] Klotz L. Active surveillance for prostate cancer: for whom? J Clin Oncol 2005;23.
[80] Jonas Hugosson GAHLPLC-GP. Results of a randomized, population-based study of biennial screening using serum prostate-specific antigen measurement to detect prostate carcinoma 2004;100:1397–405.
[81] Gao X, Porter AT, Grignon DJ, Pontes JE, Honn KV. Diagnostic and prognostic markers for human prostate cancer. Prostate 1997;31(June):264–81.
[82] Graefen M, Augustin H, Karakiewicz PI, Hammerer PG, Haese A, Palisaar J, et al. Can predictive models for prostate cancer patients derived in the United States of America be utilized in European patients? A validation study of the partin tables. Eur Urol 2003;43:6.
[83] Stephenson AJ, Kattan MW, Eastham JA, Dotan ZA, Bianco Jr FJ, Lilja H, et al. Defining biochemical recurrence of prostate cancer after radical prostatectomy: a proposal for a standardized definition. J Clin Oncol 2006;24(August):3973–8.
[84] Stephenson AJ, Scardino PT, Eastham JA, Bianco Jr FJ, Dotan ZA, DiBlasio CJ, et al. Postoperative nomogram predicting the 10-year probability of prostate cancer recurrence after radical prostatectomy. J Clin Oncol 2005;23(October):7005–12.
[85] Stephenson AJ, Scardino PT, Eastham JA, Bianco Jr FJ, Dotan ZA, Fearn PA, et al. Preoperative nomogram predicting the 10-year probability of prostate cancer recurrence after radical prostatectomy. J Natl Cancer Inst 2006;98(May):715–7.
[86] Marcelpoil R. Normalization of the minimum spanning tree. Anal Cell Pathol 1993;5(May):177–86.
[87] Albert R, Schindewolf T, Baumann I, Harms H. Three-dimensional image processing for morphometric analysis of epithelium sections. Cytometry 1992;13:759–65.
[88] Basavanhally A, Agner A, Alexe G, Ganesan S, Bhanot G, Madabhushi A. Manifold learning with graph-based features for identifying extent of lymphocytic infiltration from high grade breast cancer histology. In: MMBIA workshop in conjunction with MICCAI 2008. 2008.
[89] Basavanhally A, Xu J, Ganesan S, Madabhushi A. Computer-aided prognosis (CAP) of ER+ breast cancer histopathology and correlating survival outcome with oncotype Dx assay. In: IEEE international symposium on biomedical imaging (ISBI). 2009. p. 851–4.
[90] Doyle S, Hwang M, Shah K, Madabhushi A, Tomaszeweski J, Feldman M. Automated grading of prostate cancer using architectural and textural image features. In: International symposium biomedical imaging. 2007. p. 1284–7.
[91] Doyle S, Hwang M, Naik S, Feldman M, Tomaszeweski J. Using manifold learning for content-based image retrieval of prostate histopathology in MICCAI 2007. In: Workshop on content-based image retrieval for biomedical image archives. 2007. p. 53–62.
[92] Doyle S, Madabhushi A, Feldman M, Tomaszeweski J. A computer-aided diagnosis system for automated Gleason grading of prostatic adenocarcinoma from digitized histology advancing practice. In: Instruction and innovation through informatics (APIII). 2007.
[93] Doyle S, Hwang M, Naik S, Madabhushi A, Feldman M, Tomaszeweski J. Quantitative investigation of graph-based features for automated grading of prostate cancer. Retreat Cancer Res 2007:51.
[94] Doyle S, Agner S, Madabhushi A, Feldman M, Tomaszeweski J. Automated grading of breast cancer histopathology using spectral clustering with textural and architectural image features. In: International symposium on biomedical imaging. Paris France: IEEE; 2008. p. 496–9.
[95] Zhang L, Conejo-Garcia JR, Katsaros D, Gimotty PA, Massobrio M, Regnani G, et al. Intratumoral T cells, recurrence, and survival in epithelial ovarian cancer. N Engl J Med 2003;348(January):203–13.
[96] Sudbo J, Bankfalvi A, Bryne M, Marcelpoil R, Boysen M, Piffko J, et al. Prognostic value of graph theory-based tissue architecture analysis in carcinomas of the tongue. Lab Invest 2000;80(December):1881–9.
[97] Sudbo J, Marcelpoil R, Reith A. New algorithms based on the Voronoi Diagram applied in a pilot study on normal mucosa and carcinomas. Anal Cell Pathol 2000;21:71–86.

[98] Sudbo J, Marcelpoil R, Reith A. Caveats: numerical requirements in graph theory based quantitation of tissue architecture. Anal Cell Pathol 2000;21: 59–69.
[99] Lee G, Doyle S, Monaco J, Madabhushi A, Feldman MD, Master SR, et al. A knowledge representation framework for integration, classification of multi-scale imaging and non-imaging data: preliminary results in predicting prostate cancer recurrence by fusing mass spectrometry and histology. In: ISBI. 2009. p. 77–80.
[100] Agner S, Soman S, Libfeld E, McDonald M, Thomas K, Englander S, et al. Textural kinetics: a novel dynamic contrast-enhanced (DCE)-MRI feature for breast lesion classification. J Digit Imaging 2010.
[101] Basavanhally A, Xu J, Madabhushi A, Ganesan S. Computer-aided prognosis of ER+ breast cancer histopathology and correlating survival outcome with oncotype DX assay. In: ISBI. 2009. p. 851–4.
[102] Madabhushi A, Shi J, Rosen M, Tomaszeweski J, Feldman MD. Graph embedding to improve supervised classification and novel class detection: application to prostate cancer. MICCAI 2005;8:729–37.
[103] Basavanhally AN, Ganesan S, Agner S, Monaco JP, Feldman MD, Tomaszewski JE, et al. Computerized image-based detection and grading of lymphocytic infiltration in HER2+ breast cancer histopathology. IEEE Trans Biomed Eng 2010;57(March):642–53.
[104] A. Basavanhally, S. Ganesan, S. Agner, J. Monaco, M. Feldman, J. Tomaszewski, et al. Computerized image-based detection and grading of lymphocytic infiltration in HER2+ breast cancer histopathology. IEEE Trans Biomed Eng 2009; accepted for publication.
[105] Alexe G, Dalgin GS, Scanfeld D, Tamayo P, Mesirov JP, DeLisi C, et al. High expression of lymphocyte-associated genes in node-negative HER2+ breast cancers correlates with lower recurrence rates. Cancer Res 2007;67(November):10669–76.
[106] Gleason DF. Histologic grading of prostate cancer: a perspective. Hum Pathol 1992;23(March):273–9.
[107] Bostwick DG, Graham Jr SD, Napalkov P, Abrahamsson PA, di Sant'agnese PA, Algaba F, et al. Staging of early prostate cancer: a proposed tumor volume-based prognostic index. Urology 1993;41(May):403–11.
[108] Doyle S, Hwang M, Shah K, Madabhushi A, Feldman M, Tomaszeweski J. Automated grading of prostate cancer using architectural and textural image features. In: ISBI. 2007. p. 1284–7.
[109] Stephenson AJ, Slawin KM. The value of radiotherapy in treating recurrent prostate cancer after radical prostatectomy. Nat Clin Pract Urol 2004;1(December):90–6.
[110] Allsbrook Jr WC, Mangold KA, Johnson MH, Lane RB, Lane CG, Amin MB, et al. Interobserver reproducibility of Gleason grading of prostatic carcinoma: urologic pathologists. Hum Pathol 2001;32(January):74–80.
[111] Lexander H, Palmberg C, Auer G, Hellstrom M, Franzen B, Jornvall H, et al. Proteomic analysis of protein expression in prostate cancer. Anal Quant Cytol Histol 2005;27(October):263–72.
[112] Cooper L, Sertel O, Kong J, Lozanski G, Huang K, Gurcan M. Feature-based registration of histopathology images with different stains: an application for computerized follicular lymphoma prognosis. Comput Methods Programs Biomed 2009;96:182–93.